Purdue University
Purdue e-Pubs

Birck and NCN Publications | Birck Nanotechnology Center

4-1-2007

Nanopatterned contacts to GaN

Ho Young Kim
Birck Nanotechnology Center and Department of Physics, Purdue University, kim175@purdue.edu

P Deb
Birck Nanotechnology Center, School of Materials Engineering, Purdue University, pdeb@purdue.edu

Timothy D. Sands
Purdue University, tsands@purdue.edu

Follow this and additional works at: http://docs.lib.purdue.edu/nanopub

Kim, Ho Young; Deb, P; and Sands, Timothy D., "Nanopatterned contacts to GaN" (2007). *Birck and NCN Publications.* Paper 231.
http://docs.lib.purdue.edu/nanopub/231

This document has been made available through Purdue e-Pubs, a service of the Purdue University Libraries. Please contact epubs@purdue.edu for additional information.

Journal of ELECTRONIC MATERIALS, Vol. 36, No. 4, 2007
DOI: 10.1007/s11664-006-0050-z
© 2007 TMS

Nanopatterned Contacts to GaN

HO GYOUNG KIM,[1,4,5] PARIJAT DEB,[2,4] and TIM SANDS[2,3,4]

1.—Department of Physics, Purdue University, West Lafayette, IN 47907, USA. 2.—School of Materials Engineering, Purdue University, West Lafayette, IN 47907, USA. 3.—School of Electrical and Computer Engineering, Purdue University, West Lafayette, IN 47907, USA. 4.—Birck Nanotechnology Center, Purdue University, West Lafayette, IN 47907, USA. 5.—E-mail: kim175@purdue.edu

The effect of nanoscale patterning using a self-organized porous anodic alumina (PAA) mask on the electrical properties of ohmic and Schottky contacts to n-GaN was investigated with the aim of evaluating this approach as a method for reducing the specific contact resistance of ohmic contacts to GaN. The electrical characteristics of contacts to these nanopatterned GaN samples were compared with contacts to planar, chemically prepared ("as-grown") GaN samples and reactive ion etched (RIE) GaN films without any patterning. The specific contact resistivities to unintentionally doped n-GaN using a Ti/Al bilayer metallization were determined to be $7.4 \times 10^{-3}\ \Omega\ \mathrm{cm}^2$ for the RIE sample and $7.0 \times 10^{-4}\ \Omega\ \mathrm{cm}^2$ for the PAA patterned sample. Schottky metal contacts with Pt and Ni were prepared on the three samples to validate the effects of RIE and nanopatterning on electrical behavior. The effective barrier height was decreased and the reverse current was increased significantly in the PAA patterned sample. The radius of curvature of the nanoscale corrugation in the patterned interface was smaller than the depletion width. The reduction of the depletion width at sharp corners enhanced the local tunneling current, reducing the specific contact resistivity and decreasing the effective barrier height. These results suggest that nanopatterning with PAA on GaN can significantly lower the contact resistance.

Key words: Porous anodic alumina (PAA), contact resistance, Schottky barrier height, tunneling current

INTRODUCTION

GaN is an emerging material for applications in light-emitting devices and high-power, high-temperature, high-frequency electronic devices.[1,2] The challenges in obtaining low barrier height metal contacts for ohmic contacts to GaN have hampered the development of GaN-based devices. A large variety of elemental and multicomponent metallizations have been explored for ohmic contacts to *n*-GaN and *p*-GaN.[3–8] Additionally, various surface treatment techniques such as wet chemical surface modification,[9] dry etching,[10] and laser etching[11] have been used to reduce the ohmic contact resistance, yet specific contact resistances are still sufficiently high so as to impact device performance, particularly for *p*-GaN.

A nonlithographic technique that uses a highly ordered porous anodic alumina (PAA) template has attracted considerable interest.[12–14] The PAA patterned Si substrates have been employed as lateral epitaxial overgrowth templates for GaN films to reduce defect density.[14,15] Nanoscale Schottky contacts to *n*-Si have been found to yield a large current density that cannot be modeled as a purely thermionic emission current,[16,17] but, rather, can be explained by the enhanced tunneling due to the decrease of the Schottky barrier thickness with decreasing diode size. In addition, Chin et al.[18] proposed a simple physical model describing the current transport mechanism in Si *p-n* junctions containing silicide spikes. They explained the athermal behavior of the reverse current in terms of

(Received July 18, 2006; accepted October 27, 2006; published online February 6, 2007)

electric field enhancement at the sharp spikes and the resulting increase in tunneling current. In the present work, the role of small radius of curvature features at metal/GaN interfaces is explored by employing a PAA template as an etching mask to introduce nanoscale patterns prior to metallization. The resulting corrugated interface is shown by a combination of modeling and experiment to reduce the contact resistance by enhanced tunneling through the narrowed depletion regions surrounding the nanoscale protrusions. This new and inexpensive fabrication process for introducing nanoscale inhomogeneities into metal/GaN surfaces significantly reduces both the ohmic contact resistance and the Schottky barrier height (SBH).

EXPERIMENT

A 5-μm-thick undoped GaN film grown by hydride vapor phase epitaxy was used in this study. Unintentional donor doping yielded a net donor concentration of 8.8×10^{16} cm^{-3} at room temperature, as assessed by capacitance-voltage (C-V) measurements. The GaN sample surface was patterned using PAA as an etch mask, a detailed description of which may be found in Ref. 19. Briefly, a 60-nm-thick SiO_x film and a 1-μm-thick Al film were deposited on the GaN film by electron beam evaporation. A two-step anodization was then carried out in a 0.4 M oxalic acid solution at 4°C and a potential of 40 V, which improves the pore order in the PAA film. The sample was subjected to reactive ion etching (RIE) with etching gases of SF_6 and O_2. The hole pattern through the SiO_x film and into the GaN was generated at an etching rate of about 5 nm/min. The plasma power was 100 W and the chamber pressure was maintained at 55–60 mTorr, resulting in a dc bias of 400–425 V. The remaining alumina layer and the SiO_x layer were removed in a phosphoric acid-chromic oxide solution and buffered oxide etchant (BOE), respectively. Figure 1 show the top-view and cross-sectional view images of the PAA patterned GaN sample taken by field emission scanning electron microscopy (FESEM). The average diameter of the pores was 40 nm and the average etching depth into the GaN was about 40 nm. The density of nanopores was about 8.0×10^9 cm^{-2}, corresponding to about 10% areal coverage. The electrical characteristics of contacts to these nanopatterned GaN samples (referred to as "PAA patterned") were compared with those of as-grown GaN samples (referred to as "as-grown") and RIE etched GaN films without any patterning (referred to as "RIE etched"). The GaN samples were cleaned ultrasonically using acetone, methanol, rinsed in DI water, blown dry with N_2, and then dipped into HCl:H_2O (1:1) solution to remove the surface oxide. Circular transfer length method (CTLM) patterns[20] were defined by standard photolithography to measure the specific contact resistivity. The radius of the outer circular contact was 200 μm and the spacing between the inner and outer radii was in the range of 5 to 45 μm. Prior to metal deposition by electron-beam evaporation, all samples were dipped into BOE to remove the surface oxide. A Ti (30 nm)/Al (110 nm) bilayer was deposited by electron-beam evaporation.

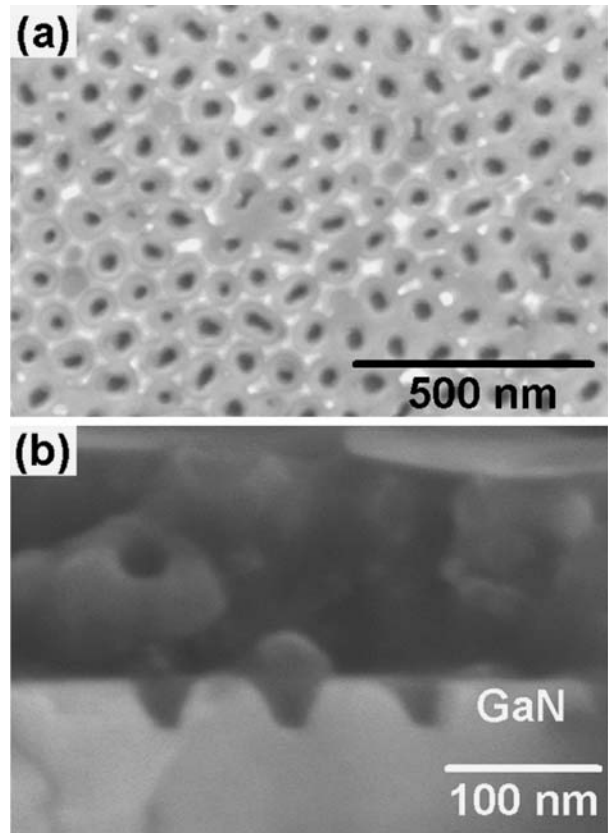

Fig. 1. FESEM images of PAA patterned GaN: (a) top view and (b) cross-sectional view. The average pore diameter is about 40 nm and the depth is about 40 nm.

To investigate the current flow mechanism across the metal-semiconductor (MS) contact, Schottky diodes were used. The samples were cleaned in acetone, methanol, and the surface oxide was removed in HCl:H_2O (1:1) solution immediately prior to loading into an electron-beam evaporator. A Ti/Al (30 nm/110 nm) bilayer was deposited over approximately half of the sample to serve as the ohmic contact, followed by rapid thermal annealing at 600°C for 1 min in an N_2 ambient. Both Pt and Ni metals with a thickness 100 nm were employed for the Schottky contact using a metal shadow mask with an exposed diameter of 250 μm. Current-voltage (I-V) and C-V measurements were performed with a Keithley 238 high current source and a HP 4275A LCR meter.

RESULTS

Figure 2 shows the I-V characteristics, measured with a gap spacing of 10 μm. The as-grown sample showed nonohmic behavior before annealing.

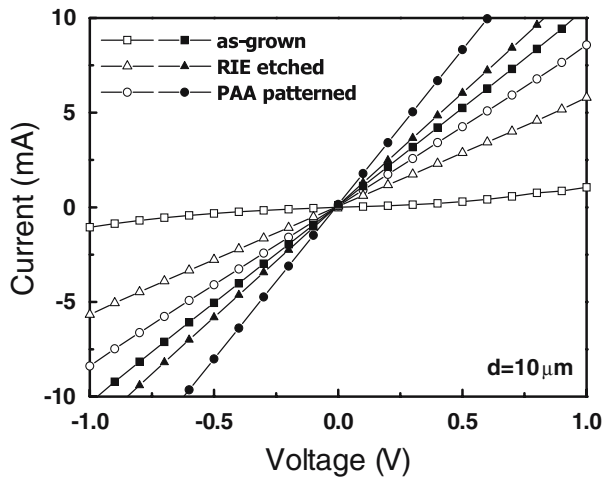

Fig. 2. I-V characteristics for Ti (30 nm)/Al (110 nm) contacts measured with a gap spacing of 10 μm (open symbol: as deposited; and solid symbol: after annealing at 600°C for 1 min in an N_2 ambient).

However, the RIE etched and PAA patterned samples yielded linear I-V characteristics. Thermal annealing at 600°C for 1 min in an N_2 ambient improved the ohmic characteristics further for all samples. To minimize the contact resistance between the probe tip and the metal layer, a four-point probe configuration was used to measure the total resistance between the inner and outer circular contacts. The specific contact resistivities for as-deposited samples were determined to be 7.4 $(\pm 1.6) \times 10^{-3}$ Ω cm^2 for the RIE etched sample and 7.0 $(\pm 1.3) \times 10^{-4}$ Ω cm^2 for the PAA patterned sample, respectively. The specific contact resistivities for annealed samples were estimated to be 3.8 $(\pm 1.4) \times 10^{-4}$ Ω cm^2 for the as-grown sample, 1.7 $(\pm 0.7) \times 10^{-4}$ Ω cm^2 for the RIE etched sample and 9.2 $(\pm 1.5) \times 10^{-5}$ Ω cm^2 for the PAA patterned sample, respectively. The RIE etching lowered the contact resistance, an effect which has been attributed to the increased electron concentration near the GaN surface[10] resulting from the introduction of etching-induced nitrogen vacancies (V_N) that act as donors.[21,22] The contact resistance was decreased further in the PAA patterned sample. The presence of nanoscale corrugation in the GaN reduced the contact resistivity significantly. The mechanism of the improved electrical properties with nanoscale patterning was investigated further using Schottky diodes.

The forward bias characteristics of a Schottky diode can be analyzed using the thermionic emission model:[23]

$$I = I_0[\exp\{q(V - IR_S)/n\mathrm{k_B}T\} - 1] \quad (1)$$

$$I_0 = AA^{**}T^2 \exp(-q\phi_B/\mathrm{k_B}T) \quad (2)$$

where A is the device area; A^{**} is the effective Richardson constant, taken to be 26.4 A/cm^{2}K^2 for n-GaN;[24] ϕ_B is the barrier height; n is the ideality factor; V is the applied voltage; and R_S is the series resistance. Figure 3 shows the current density-voltage (J-V) characteristics with Pt and Ni contacts, and the extracted electrical parameters are tabulated in Table I. The effective SBHs for the Pt contacts were determined to be 0.98 eV, 0.52 eV, and 0.49 eV for the as-grown sample, the RIE etched sample and the PAA patterned sample, respectively. The effective SBHs for the Ni contacts were determined to be 0.86 eV, 0.51 eV, and 0.46 eV for the as-grown sample, the RIE etched sample and the PAA patterned sample, respectively. Choi et al.[25] observed significant reduction of the SBH in Pt/n-GaN from 1.0 eV for the as-grown sample to 0.43 eV for the inductively coupled plasma (ICP) etched sample. Based on deep level transient spectroscopy (DLTS) studies, they suggested that ICP etching produced V_N- or V_N-related deep levels, which act as a conducting path that lowers the effective energy barrier. The same behavior is likely to be responsible for the degradation in electrical properties of the RIE etched Schottky diodes prepared and characterized in the present work.

Compared to the RIE etched sample, the PAA patterned sample yielded a lower barrier height and a higher reverse current. The PAA patterned interface can be regarded as a combination of two regions: (1) an unpatterned region (high barrier height region) and (2) a patterned region (metal-filled nanopores). The total current through the MS interface was analyzed according to the parallel conduction model, which is given by[26]

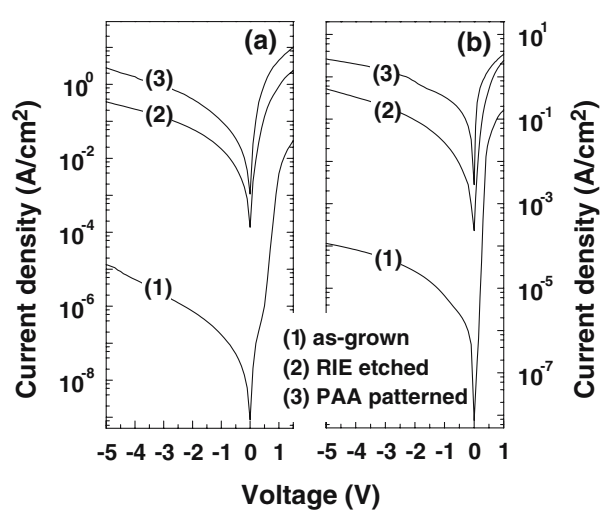

Fig. 3. I-V characteristics of (a) Pt/n-GaN Schottky contacts and (b) Ni/n-GaN Schottky contacts.

Table I. Electrical Parameters Obtained from Schottky Diodes to *n*-GaN with Pt and Ni Contacts

Sample	Schottky Contact Metal	Ideality Factor (n)	$q\phi_B$ (eV)	N_D (cm^{-3})
As grown	Pt	1.32	0.98	8.8×10^{16}
	Ni	1.46	0.86	
RIE etched	Pt	1.78	0.52	1.6×10^{17}
	Ni	1.75	0.51	
PAA patterned	Pt	1.93	0.49	2.2×10^{17}
	Ni	1.98	0.46	

$$\phi_C = -\frac{k_B T}{q} \ln \left\{ \frac{S_l}{S} \left[\exp\left(-\frac{q\phi_l}{k_B T}\right) - \exp\left(-\frac{q\phi_h}{k_B T}\right) \right] + \exp\left(-\frac{q\phi_h}{k_B T}\right) \right\} \quad (3)$$

where S_l is the area of low barrier phase, ϕ_h is the high barrier height, ϕ_l is the low barrier height, and ϕ_C is the effective barrier height. Figure 4 shows the calculated curves of effective barrier height versus areal fraction of low barrier phase (S_l/S). The SBHs determined from the as-grown Pt and Ni Schottky contacts were used as high barrier heights. The expected barrier heights for the PAA patterned samples (areal fraction of 0.1) were about 0.58 eV for the Pt contact and 0.57 eV for the Ni contact. These expected values are, however, higher than the effective barrier heights obtained for the PAA patterned samples. Thus, the simple parallel conduction model cannot explain the current transport across the corrugated MS interface.

DISCUSSION

The current transport across nanoscale features in a MS interface can be obtained by solving the Poisson equation numerically. When there is symmetry of coordinates, however, an analytical solution may be possible. A metal contact in a nanoprotrusion can be regarded as a half-immersed sphere (denoted as "immersed sphere"). The effective radius (r_{eff}) of a hemispherical metallic nanoprotrusion with volume equal to the estimated volume of the typical nanoprotrusion (Fig. 1) is 20–25 nm. The potential distribution within the depletion region surrounding a metal sphere of radius r embedded in the semiconductor (denoted as "embedded sphere") is[16]

$$\varphi(x) = \frac{qN_d}{3\varepsilon_s} \left(\frac{3(r+w)^2}{2} - \frac{(r+w)^3}{(r+x)} - \frac{(r+x)^2}{2} \right) \quad (4)$$

where x is the radial distance from the surface of the embedded sphere ($0 \le x \le w$), N_d is the carrier concentration, and w is the depletion width. Equation 4 satisfies the following boundary conditions: (1) the potential in the semiconductor bulk is zero; and (2) the potential on the surface of the sphere is V_S, where V_S is the potential difference over the depletion region, which can be given by $V_S = (q\phi_B - \psi_F)/q - V$, where ψ_F is the energy difference between the conduction band and Fermi level. The same potential profile as Eq. 4 can be used for the immersed sphere. It is noted that the contact area, hence, the total current across the immersed sphere, is one half that of the embedded sphere.

The mechanism of the current transport across a nanoprotrusion was evaluated analytically using the following method. The standard J-V relationship is[27,28]

$$J = \frac{2q}{h} \int_0^\infty T(E, k_{||}) dE \left[\int \frac{d^2 k_{||}}{(2\pi)^2} (f(E - qV) - f(E)) \right] \quad (5)$$

Here, E is the energy above the semiconductor conduction band edge, which satisfies $E = E_x + E_{||}$, where x and $||$ are the normal and parallel direction (y and z) to the MS interface, respectively; T is the transmission coefficient obtained from the Wenstzel–Kramers–Brillouin (WKB) approximation;[27] and f is the Fermi–Dirac distribution function. The expression in the brackets of Eq. 5 can be given by, after analytical treatment,[27,28]

$$n(E_x) = \frac{2\pi m^* k_B T}{h^2} \ln \left[\frac{1 + \exp[(E_F - E_x + qV)/k_B T]}{1 + \exp[(E_F - E_x)/k_B T]} \right] \quad (6)$$

Therefore, J can be written simply as

$$J = \frac{2q}{h} \int_0^\infty dE_x T(E_x) n(E_x) \quad (7)$$

Current transport across the MS contact can be thought of as the sum of the tunneling component (when the electron energy is below the maximum of the potential) and the thermionic emission component (when the electron energy is above the maximum of the potential).

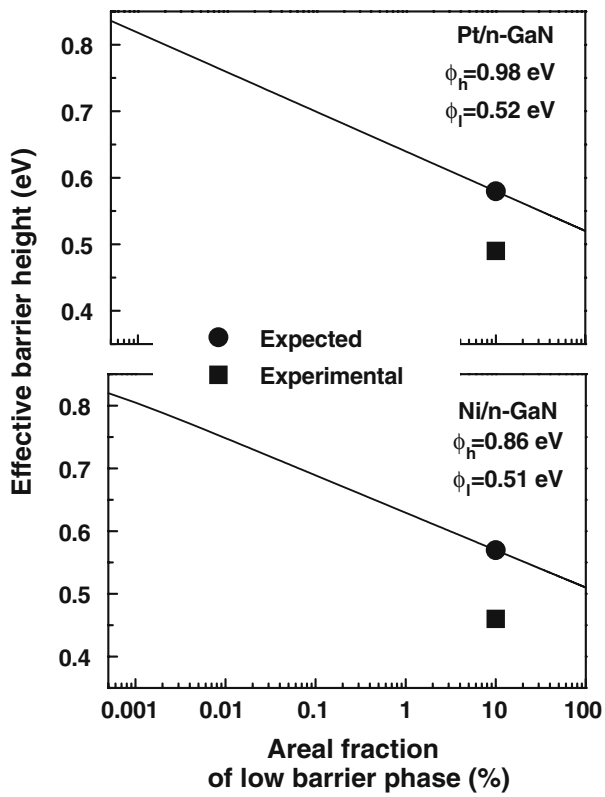

Fig. 4. Calculated effective barrier height versus the areal fraction of low barrier phase using the parallel conduction model. The expected barrier height (solid circle) and obtained barrier height (solid square) for the PAA patterned sample are also presented.

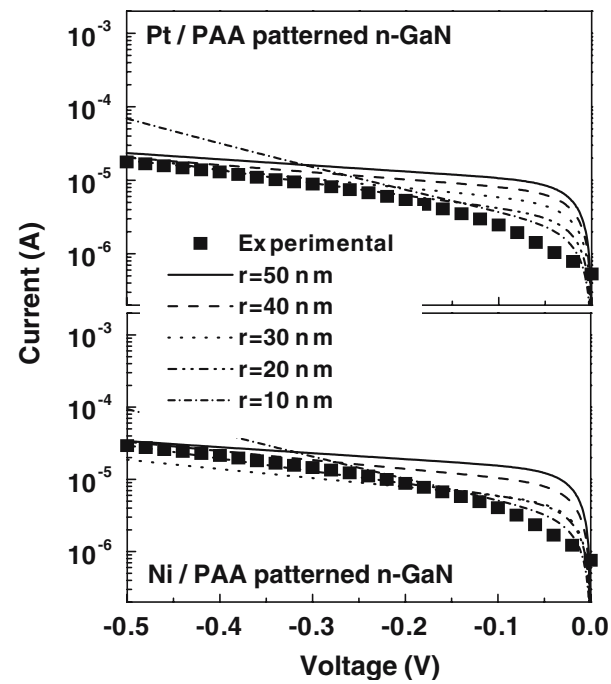

Fig. 5. Experimental and simulated reverse I-V characteristics for the PAA patterned GaN.

Since nanopores were patterned on the GaN surface by RIE etching, the barrier heights obtained from the RIE etched samples and the barrier heights obtained from the as-grown samples were used for the patterned region and the unpatterned region, respectively. In addition, the contact area of one nanopore was calculated as $2\pi r^2$, where r is the radius of the immersed sphere. It should be noted, however, that the SBH of the sidewalls of a nanoprotrusion may be different than the SBH of the RIE etched sample due to the different crystallographic orientation, as may be inferred from the dependence of the SBH on the polarity of the basal plane surface.[29] For simplicity, an orientation-independent SBH was assumed for the nanoprotrusion. The total current values for the PAA patterned sample were calculated by summing the current across the nanoprotrusion and the current across the unpatterned region. Figure 5 shows the experimental and simulated reverse I-V characteristics of the PAA patterned samples. The radius of the nanoprotrusion was changed from 10 nm to 50 nm, while the density of nanoprotrusions ($8.0 \times 10^9\ \mathrm{cm}^{-2}$) and the metal contact area (250 μm in diameter) were held constant. A radius of 10 nm yields higher calculated current values than those of other radii, which is expected due to the higher tunneling current corresponding to the smaller radius of the nanoprotrusion. The values of the radius in the range of 20–30 nm provide a reasonable fit to the experimental data, in agreement with the measured nanoprotrusion radius of about 20–25 nm. Consequently, the current transport modeling presented here can explain the reverse current characteristics of PAA patterned samples.

When current transport is controlled by thermionic field emission (TFE), the relationship between the current and voltage can be expressed by[30]

$$I = I_0 \exp(qV/E_0) \tag{8}$$

$$I_0 = \frac{AA^*[\pi E_{00} q(\phi_B - V - \psi_F)]^{1/2}}{\mathrm{k_B}\cosh(E_{00}/\mathrm{k_B}T)} \times \exp\left(-\frac{q\psi_F}{\mathrm{k_B}T} - \frac{q(\phi_B - \psi_F)}{E_0}\right) \tag{9}$$

with

$$n_{\mathrm{tunn}} = \frac{qE_{00}}{\mathrm{k_B}T}\exp\left(\frac{qE_{00}}{\mathrm{k_B}T}\right) = \frac{qE_0}{\mathrm{k_B}T} \tag{10}$$

where E_{00} is the characteristic energy related to the tunneling probability, given by

$$E_{00} = \frac{qh}{4\pi}\left(\frac{N_D}{m^*\varepsilon_S}\right)^{1/2} \quad (11)$$

Current transport across the nanoprotrusion interface was simulated with the values obtained from the RIE etched samples, shown in Table 1, and analyzed using Eqs. 8–11 to study the effect of the radius of the nanoprotrusion on the effective barrier height and the ideality factor. Figure 6 shows the effective barrier height and the ideality factor versus radius of the nanoprotrusion. This figure shows that, as the radius of the nanoprotrusion decreases, the effective barrier height decreases while the ideality factor increases. A similar behavior was observed in a previous study describing nanoscale contacts to GaAs.[31] This result might explain the lower barrier height and higher ideality factor of the PAA patterned samples compared to those of the RIE etched samples. As presented in Table 1 for the RIE etched samples, ideality factors were measured to be 1.78 for the Pt contact and 1.75 for the Ni contact. These large values imply that RIE etched samples yield current components other than thermionic emission current, such as tunneling current due to the RIE-induced traps at the interface, as mentioned previously.

The simulated forward current values from the nanoprotrusion for the values of the radius in the range of 10 to 50 nm have been found to be higher than those from the unpatterned region by more than four orders of magnitude when the forward bias is varied from 0 V to 0.3 V. As a result, the current values from the unpatterned region can be negligible and the current values from the nanoprotrusion were considered to investigate the forward I-V characteristics of the PAA patterned samples. The simulated current values can be described by

$$I_1 = I_0[\exp(qV/k_BT) - 1] \quad (12)$$

To account for the nonideality of the RIE etched samples, the ideality factors of the RIE etched samples were included and the I-V characteristics can be given by

$$I_2 = I_0[\exp(nqV/k_BT) - 1] \quad (13)$$

where n is the ideality factor obtained from the RIE etched samples. Using Eq. 12, Eq. 13 can be written as

$$I_2 = I_1[\exp(qV/k_BT) - 1][\exp(qV/k_BT) - 1]^{-1} \quad (14)$$

Figure 7 shows the experimental and simulated forward I-V characteristics of the PAA patterned samples with various nanoprotrusion radii according to Eq. 14. For the Pt contact, the radius of 15–20 nm shows the best agreement with the experimental data, while the radius of 20–25 nm gives the best fit for the Ni contact. These values are similar to the values obtained from the fitting to the reverse I-V characteristics. Thus, it can be inferred that the current transport model employed in this study explains both the forward and reverse I-V characteristics for the PAA patterned samples. Figure 8 shows schematic diagrams of the current transport under the reverse bias across the MS interface. For the RIE etched sample, the current mechanism is a combination of (i) thermionic emission transport over the Schottky barrier and (ii)

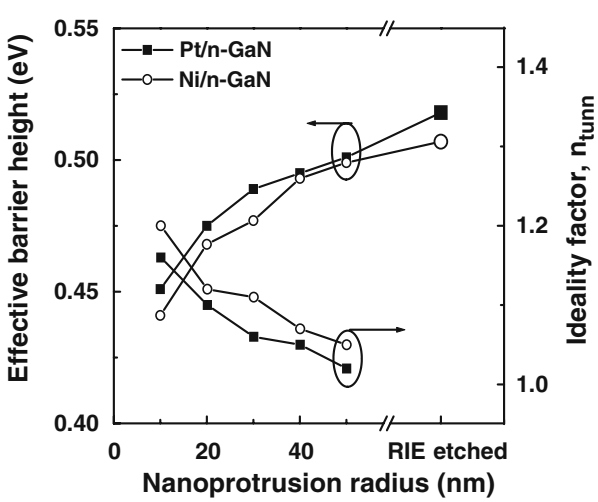

Fig. 6. Effective barrier height and ideality factor versus radius of the nanoprotrusion.

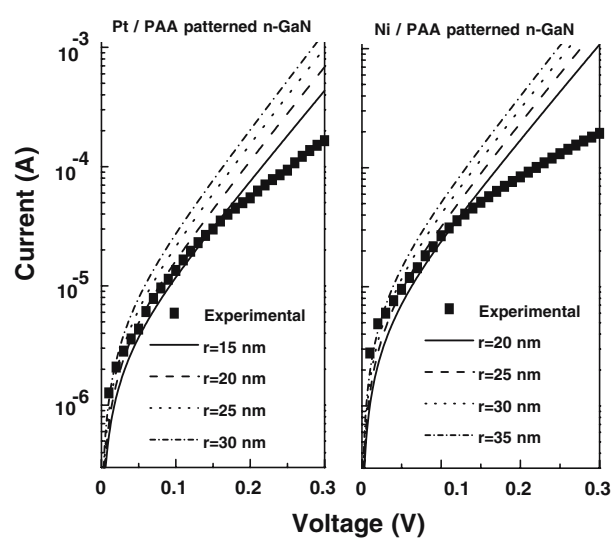

Fig. 7. Experimental and simulated forward I-V characteristics with the experimentally determined ideality factor from the RIE etched sample.

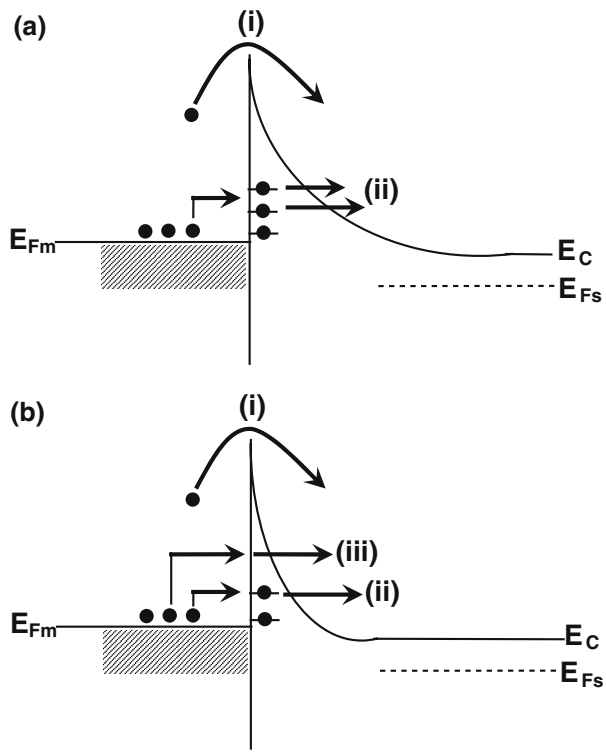

Fig. 8. Schematic diagram of electron transport across the MS interface for (a) the RIE etched sample and (b) the PAA patterned sample across the nanoprotrusion.

trap-assisted tunneling caused by RIE etching, as shown in Fig. 8a. After PAA patterning, the barrier thickness was reduced due to the small radius of curvature of the nanoprotrusions. Therefore, the transport of electronic charge across the PAA patterned interface also includes a component due to the direct tunneling across the thinned depletion region, as depicted in Fig. 8b.

The effect of the radius of the nanoprotrusions on the contact resistance for Ti/Al metallization was studied in more detail. The barrier heights for the RIE etched and the PAA patterned samples were obtained with the I-V method, which utilizes a large-area contact and reverse-biased I-V characteristics.[32] The barrier heights were found to be 0.44 eV for the as-grown sample, 0.37 eV for the RIE etched sample, and 0.35 eV for the PAA patterned sample. The total current for the PAA patterned sample was assumed to be the sum of the current across the nanoprotrusions and the current across the unpatterned region, as mentioned previously. The fractional areal coverage of the patterned nanoprotrusions was set at 0.1. The total current can be given as

$$I = (AA_n d)J_n + 0.9AJ_u \tag{15}$$

where A is the device area, d is the density of nanopores, A_n is the outer surface area of nanoprotrusion ($2\pi r^2$), J_n is the current density through the nanoprotrusion, and J_u is the current density through the unpatterned region. Considering the differential conductance given by

$$dJ/dV = (A_n d)dJ_n/dV + 0.9\, dJ_u/dV \tag{16}$$

By the definition of zero differential conductance, this expression can be converted to

$$\rho_c^{-1} = (A_n d)\rho_{cn}^{-1} + 0.9\rho_{cu}^{-1} \tag{17}$$

For the carrier concentration of 8.8×10^{16} cm^{-3} in the as-grown sample, E_{00} is calculated to be 3.7 meV according to Eq. 11 and E_{00}/k_BT is 0.14 at T = 300 K. Because E_{00}/k_BT is smaller than unity, thermionic emission (TE) is the dominant current mechanism for the as-grown sample. As a result, the specific contact resistivity of the as-grown sample was obtained from the current transport theory in the TE regime,[33] given as

$$\rho_{cu} = \frac{k_B}{qA^{**}T}\exp\left(\frac{q\phi_B}{k_BT}\right) \tag{18}$$

From Eq. 7, the specific contact resistivity of a nanoprotrusion, ρ_{cn}, can be written as

$$\rho_{cn}^{-1} = \frac{4\pi m^* q^2}{h^3}\int_0^\infty dE_x T(E_x)\frac{1}{1+\exp[(E_x - E_F)/k_BT]} \tag{19}$$

Figure 9 shows the simulated specific contact resistivity versus radius of the nanoprotrusion for several barrier heights. In all cases, as the radius of the nanoprotrusion increases, the contact resistivity approaches a constant value. In this limit, the size effect of the nanoprotrusion is less prominent, and current transport depends mainly on the barrier height. On the other hand, as the radius of the nanoprotrusion decreases, a remarkable reduction of contact resistivity is observed due to the enhanced electric field. As shown in Fig. 9, an experimentally obtained value of 7.0×10^{-4} Ω cm^2 was well matched to the model for a barrier height of 0.31 eV for the RIE etched sample and a nanoprotrusion radius of 20 nm. These extracted values are not exactly the same as the obtained values of the barrier height of the RIE etched sample (0.37 eV) and the radius of the nanoprotrusion (20–30 nm from fitting the I-V characteristics from Pt and Ni contacts), but the results clearly indicate that the contact resistance was reduced significantly due to the enhanced tunneling current arising from the small radius of curvature of the nanoprotrusions. Note that, throughout this study, the current

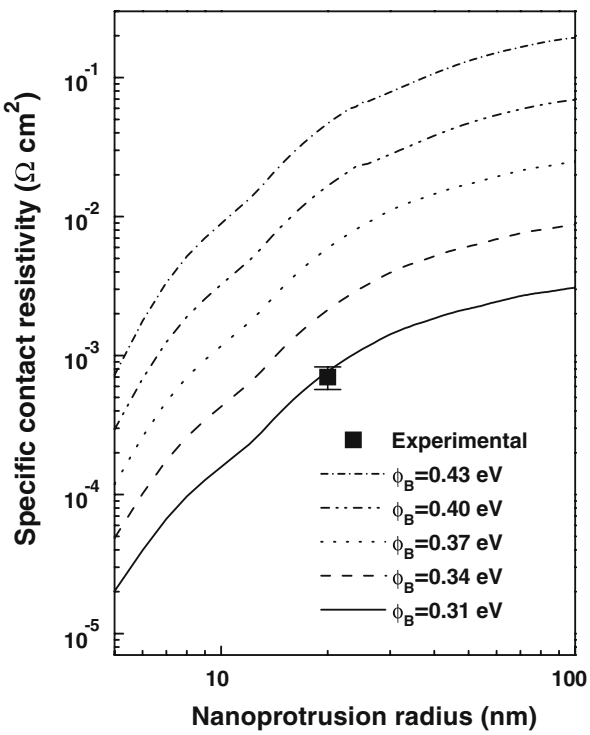

Fig. 9. Simulated specific contact resistivity versus radius of the nanoprotrusion with constant areal coverage of 10% for n-GaN.

transport was modeled as a sum of current through two different regions (patterned and unpatterned). Thus, the effect of the potential discontinuity at the boundary, which will also provide another source of current transport, was not included. To include these boundary effects, numerical approaches are necessary. However, the good agreement between the analytical models presented here and the experimental results suggest that more complex models are not needed.

CONCLUSIONS

The effect of nanopatterning on contacts to n-GaN using porous anodic alumina (PAA) films as masks has been studied. Nonlinear I-V characteristics for the as-grown samples became linear for the RIE etched and PAA patterned samples. Significant reduction of the specific contact resistivity was observed for the PAA patterned sample. Investigation of the current transport mechanism in Schottky metal contacts with Pt and Ni using I-V measurements along with simulation revealed that the effective barrier height was decreased and the reverse current was increased significantly in the PAA patterned sample. Reduction of the depletion width around the nanoprotrusion resulted in an enhanced local tunneling current, thereby reducing the specific contact resistivity and decreasing the effective barrier height. Although the experimental focus of the work presented here is on contacts to n-GaN, a comparable lowering of the specific contact resistivity to nanopatterned contacts to p-GaN is expected.

ACKNOWLDGEMENT

This work was supported by the National Science Foundation (Grant No. ECS-0424161).

REFERENCES

1. S. Nakamura, G. Fasol, *The Blue Laser Diode* (Berlin: Springer, 1997).
2. S.J. Pearton, J.C. Zolper, R.J. Shul, and F. Ren, *J. Appl. Phys.* 86, 1 (1999).
3. S. Ruvimov, Z. Liliental-Weber, J. Washburn, K.J. Duxstad, E.E. Haller, S.N. Mohammad, Z. Fan, and H. Morkoç, *Appl. Phys. Lett.* 69, 1556 (1996).
4. J.K. Sheu, Y.K. Su, G.C. Chi, M.J Jou, C.C. Liu, C.M. Chang, W.C. Hung, J.S. Bow, and Y.C. Yu, *J. Vac. Sci. Technol. B* 18, 729 (2000).
5. N.A. Papanicolaou, M.V. Rao, J. Mittereder, and W.T. Anderson, *J. Vac. Sci. Technol. B* 19, 261 (2001).
6. J.-K. Ho, C.-S. Jong, C.C. Chiu, C.N. Hunag, C.-Y. Chen, and K.K. Shih, *Appl. Phys. Lett.* 74, 1275 (1999).
7. C.-F. Chu, C.C. Yu, Y.K. Wang, J.Y. Tsai, F.I. Lai, and S.C Wang, *Appl. Phys. Lett.* 77, 3423 (2000).
8. L. Zhou, W. Lanford, A.T. Ping, I. Adesida, J.W. Yang, and A. Khan, *Appl. Phys. Lett.* 76, 3451 (2000).
9. C.-T. Lee, Y.-J. Lin, and C.-H. Lin, *J. Appl. Phys.* 92, 3825 (2002).
10. Z. Fan, S.N. Mohammad, W. Kim, Ö. Aktas, A.E. Botchkarev, and H. Morkoç, *Appl. Phys. Lett.* 68, 1672 (1996).
11. H.W. Jang, T. Sands, and J.-L. Lee, *J. Appl. Phys.* 94, 3529 (2003).
12. D. Crouse, Y.H. Lo, A.E. Miller, and M. Course, *Appl. Phys. Lett.* 76, 49 (1999).
13. Y. Kanamori, K. Hane, H. Sai, and H. Yugami, *Appl. Phys. Lett.* 78, 142 (2001).
14. J. Liang, S.K. Hong, N. Kouklin, R. Beresford, and J.M. Xu, *Appl. Phys. Lett.* 83, 1752 (2003).
15. Y.D. Wang, K.Y. Zang, S.J. Chua, S. Tripathy, P. Chen, and C.G. Fonstad, *Appl. Phys. Lett.* 87, 251915 (2005).
16. G.D.J. Smit, S. Rogge, and T.M. Klapwijk, *Appl. Phys. Lett.* 81, 3852 (2002).
17. M. Hugelmann and W. Schindler, *Appl. Phys. Lett.* 85, 3608 (2004).
18. D.Z. Chi, W.D. Wang, S.J. Chua, and S. Ashok, *J. Appl. Phys.* 92, 7532 (2002).
19. P. Deb, H. Kim, V. Rawat, M. Oliver, S. Kim, M. Marshall, E. Stach, and T. Sands, *Nano Lett.* 5, 1847 (2005).
20. D.K. Schroder *Semiconductor Material and Device Characterization* (Wiley, New York, 1998, pp. 147–159).
21. J. Neugebauer and C.G. Van de Walle, *Phys. Rev. B* 50, 8067 (1994).
22. C. Wetzel, T. Suski, J.W. Ager III, E.R. Weber, E.E. Haller, S. Fischer, B.K. Meyer, R.J. Molnar, and P. Perlin, *Phys. Rev. Lett.* 78, 3923 (1997).
23. S.M. Sze, *Physics of Semiconductor Devices* (Wiley, New York, 1981, pp. 245–297).
24. S. Strite and H. Morkoc, *J. Vac. Sci. Technol. B* 10, 1237 (1992).
25. K.J. Choi, H.W. Jang, and J.-L Lee, *Appl. Phys. Lett.* 82, 1233 (2003).
26. I. Ohdomari and K.N. Tu, *J. Appl. Phys.* 51, 3735 (1980).
27. J.H. Davies, *The Physics of Low Dimensional Semiconductors* (Cambridge University Press, Cambridge, United Kingdom, 1998, pp. 162–172).
28. D.K. Ferry and S.M. Goodnick, *Transport in Nanostructures* (Cambridge University Press, Cambridge, United Kingdom, 1997, pp. 114–118).

29. U. Karrer, O. Ambacher, and M. Stutzmann, *Appl. Phys. Lett.* 77, 2012 (2000).
30. E.H. Rhoderick, R.H. Williams, *Metal Semiconductor Contacts* (Oxford, United Kingdom: Clarendon, 1988).
31. N.V. Vostokov and V.I. Shashkin, *JETP* 99, 211 (2004).
32. T. Mori, T. Kozawa, T. Ohwaki, Y. Taga, S. Nagai, S. Yamasaki, S. Asami, N. Shibata, and M. Koike, *Appl. Phys. Lett.* 69, 3537 (1996).
33. A.Y.C. Yu, *Solid-State Electron.* 13, 239 (1970).